International Journal on Magnetic Particle Imaging
Vol 8, No 2, Article ID 2212002, 8 Pages

Infinite Science Publishing

Research Article

Joint multi-patch reconstruction: fast and improved results by stochastic optimization

Lena Zdun [a,*] · Marija Boberg [b,c] · Christina Brandt [a]

[a] Department of Mathematics, Universität Hamburg, Hamburg, Germany
[b] Section for Biomedical Imaging, University Medical Center Hamburg-Eppendorf, Hamburg, Germany
[c] Institute for Biomedical Imaging, Hamburg University of Technology, Hamburg, Germany
[*] Corresponding author, email: lena.zdun@uni-hamburg.de

Received 23 March 2022; Accepted 28 November 2022; Published online 22 December 2022

© 2022 Zdun *et al.*; licensee Infinite Science Publishing GmbH

This is an Open Access article distributed under the terms of the Creative Commons Attribution License (http://creativecommons.org/licenses/by/4.0), which permits unrestricted use, distribution, and reproduction in any medium, provided the original work is properly cited.

Abstract

In order to measure larger volumes in magnetic particle imaging, it is necessary to divide the region of interest into several patches and measure those patches individually due to a limited size of the field of view. This procedure yields truncation artifacts at the patches boundaries during reconstruction. Applying a regularization which takes into account neighbourhood structures not only on one patch but across all patches can significantly reduce those artifacts. However, the current state-of-the-art reconstruction method using the Kaczmarz algorithm is limited to Tikhonov regularization. We thus propose to use the stochastic primal-dual hybrid gradient method to solve the multi-patch reconstruction task. Our experiments show that the quality of our reconstructions is significantly higher than those obtained by Tikhonov regularization and Kaczmarz method. Moreover, using our proposed method, a joint reconstruction considerably reduces the computational costs compared to multiple single-patch reconstructions. The algorithm proposed is thus competitive to the current state-of-the-art method not only regarding reconstruction quality but also concerning the computational effort.

I. Introduction

The relation between the particle distribution and the received signal in magnetic particle imaging (MPI) can be described by a linear operator. We thus have to solve an ill-posed linear system to reconstruct a magnetic particle image. The discrete inverse problem is of the form

$$Sc = u,$$

where $S \in \mathbb{R}^{2K\times N}$ is the measured forward operator, i.e. the system matrix of MPI in the frequency domain, $c \in \mathbb{R}^N$ is the unknown concentration to be recovered and $u \in \mathbb{R}^{2K}$ contains the Fourier coefficients of the received signal. By N we denote the number of points measured in space and K is the number of frequencies. Note that we split the matrix and the data into their real and imaginary parts to be able to exploit the structure of our algorithm and reduce the computational complexity of each iteration step.

Due to physiological constraints, the covered field of view (FOV) in MPI is limited to a few cubic centimeters. To be more precise, the size of the field of view is proportional to the quotient of the drive-field amplitude and the gradient strength. It can thus be enlarged either by lowering the gradient strength, which leads to a loss of resolution [1], or by increasing the drive-field amplitude. However, the amplitude is limited by power loss, tissue heating [2] and peripheral nerve stimulation [3, 4]. It is thus necessary to perform multi-patch measurements to capture a larger volume. For that purpose, additional low frequency focus fields are used to continuously or step-wise relocate the area covered by the field-free point

(FFP). In this work, we only consider the static focus field approach, where the FFP trajectory center is shifted in between individual measuring sequences. The total region of interest can then by seen as a patchwork of the FOVs at different positions. We thus call the FOV covered at a certain FFP position a patch.
Reconstruction of multi-patch data is an important field of research and various approaches have been proposed. First of all, one can combine patch-wise reconstructions in a post-processing step [5]. When reconstructing drive-field patches separately, artifacts at the borders occur as well as stripe artifacts, when overlapping measurements are taken [6]. Joint reconstruction of the different patches yields artifact-reduced images, but the need of storing one system matrix (SM) measured on the full FOV, i.e. over all patches, per patch poses huge memory requirements and is very time-consuming in the calibration process [7]. Exploiting the sparsity of that joint system matrix and reusing a single calibration scan reduces the computational effort from scaling quadratically with the number of patches to scaling linearly [8]. However, to apply that approach shift invariance of the system matrices has to be assumed, which holds only for ideal magnetic fields, but has to be generalized for large field imperfections. Boberg et. al. perform this generalization by applying a clustering in similar matrices, where within each cluster the shift invariance holds in good approximation [9]. In [10] the authors propose to use the approximation error method in order to model the truncation error at the patches' boundaries. This allows for single patch reconstructions or could be combined with the previous approaches.

In this work, we do not focus on how to efficiently measure, store and process system matrices but we focus on reconstruction algorithms. Solving the linear problem with direct methods comes with a cubic complexity, which is not sufficient to reach real-time reconstruction even in the single patch case [11]. Iterative methods, in contrast, rely on matrix-vector multiplications and thus have only quadratic complexity, which make them a lot more favorable in MPI reconstruction. The state-of-the-art reconstruction method in Lissajous-type MPI is the Kaczmarz method combined with Tikhonov regularization and a non-negativity constraint. The Kaczmarz method provides a very fast convergence for solving the MPI imaging equation [11–13]. To allow a more flexible regularization various reconstruction algorithms based on modern splitting approaches using proximity operators such as ADMM [14–16], forward-backward splitting [17] and primal-dual splitting [18] have been proposed for single-patch MPI reconstructions. In [16], the ADMM method uses Kaczmarz method to solve the occurring subproblems, which obviously results in a longer runtime than Kaczmarz method combined with early stopping. However, it is shown to outperform a lot of algorithms as the CG method, (forward-backward) splitting methods [17, 19] and FISTA [20] regarding the computational costs. So far, none of the proposed algorithms was applied to the multi-patch case except for Kaczmarz's method. The main drawback is the memory consumption of the large multi-patch system matrix and, where necessary, the computation of the normal matrix $S^T S$.
It is not surprising that a fast and effective reconstruction gets more important the larger the data sets get. An exemplary 3D single-patch system matrix with 20,000 rows corresponding to the selected frequencies and $30^3 = 27{,}000$ columns corresponding to the voxels would grow to a joint system matrix with 120,000 rows and about 135,000 columns for a setup with 6 patches with a slight overlap. The huge system matrix has to be held in memory for most algorithmic approaches, which is often unfeasible, whereas Kaczmarz method is a row-action algorithm that uses one row per inner iteration only. The above mentioned algorithms cannot challenge Kaczmarz method in terms of runtime in a single patch setting and as their costs depend on the size of the system matrix, they will not be competitive in a joint multi-patch reconstruction setting with a much larger system matrix.

We thus propose a joint reconstruction by the stochastic primal-dual hybrid gradient (SPDHG) method allowing for various different regularization terms. SPDHG is a stochastic variant of the Chambolle-Pock algorithm, belonging to the class of primal-dual splitting approaches, and has been proposed in 2018 [21]. It has been recently adapted for MPI and thanks to system-matrix splitting showed a similar reconstruction quality by the same runtime as the Kaczmarz method [18]. Regarding memory consumption, we denote that the system matrix can be split row-wise into smaller parts as to reduce the size of the matrix to hold in memory.

The aim of this work is twofold: for one thing, we show that neighborhood respecting regularization terms significantly improve the quality of reconstructed magnetic particle images in a multi-patch setting. Moreover, we demonstrate that the SPDHG algorithm can solve those more sophisticated optimization problems fast enough to be competitive to the current state-of-the-art multi-patch MPI reconstruction method.
Note that this paper is an extension of the IWMPI 2022 abstract [22], as such, some of the results have already been published in that abstract and some parts of this work are similar. However, there are important differences. First, in this work we pay more attention to the details of the considered optimization problems and algorithm. Second, we have added an additional comparison to the joint Kaczmarz method, which we study with a more detailed analysis, and results from measurement data.

The remainder of this work is organized as follows: we introduce different single patch and joint reconstruction algorithms and state the corresponding optimization problems in Section II. Following this, we outline the data used for numerical experiments and start a detailed

 © 2022 Infinite Science Publishing

numerical comparison of the approaches in Section III. We end with a conclusion and discuss future research directions.

II. Methods

II.I. Reconstruction algorithms

Assume that the total FOV Ω^{SF} covered by the system matrices (SM) is divided into L patches Ω_l^{SF}, $l \in \{1, ..., L\}$ with overlapping parts. We acquire one system matrix S_l per patch, which is measured on that patch only instead of the full FOV, reducing the memory requirements but as a quid pro quo yielding convolution artifacts. The measurements for patch l are stored in u_l for $l \in \{1, ..., L\}$, such that the L imaging equations are given by

$$S_l c_l = u_l \quad \forall l \in \{1, ..., L\}, \tag{1}$$

where c_l contains the concentration of the l-th patch. Note that these equations are coupled through the overlap of the SM FOVs, i.e. $\Omega_l^{\mathrm{SF}} \cap \Omega_j^{\mathrm{SF}} \neq \emptyset$ for some $l \neq j$. The reconstruction task can either be solved by a single patch (SP) or by a joint (J) approach.

II.I.1. Single patch reconstruction

The SP approach is straightforward: each equation in (1) is solved independently and the concentrations c_l on the different patches are then stacked together in a post-processing step. Various weighting strategies are easily conceivable and have been compared [5]. We use a fade-in/fade-out approach, i.e. a linear weighting, as this reduces artifacts occurring at the patches boundaries and overlapping parts. While it is advantageous that only one SM needs to be held in memory during each reconstruction process, the stacked reconstructions typically suffer from severe stripe and border artifacts. The intensity of those artifacts can differ depending on the applied regularization. For comparison purposes, we consider two different SP reconstructions. The first one is obtained by the state-of-the-art Kaczmarz method with Tikhonov and iterative regularization (i.e. early stopping), using an ℓ^2 data fitting term, solving

$$\min_{c_l \geq 0} \lambda \|c_l\|_2^2 + \frac{1}{2} \|S_l c_l - u_l\|_2^2 \quad \forall l \in \{1, ..., L\}. \tag{2}$$

The second one is obtained by SPDHG method with non-negative fused lasso (FL) regularization and ℓ^1 data fitting, i.e. solving

$$\min_{c_l \geq 0} \alpha \mathrm{TV}(c_l) + \beta \|c_l\|_1 + \|S_l c_l - u_l\|_1 \quad \forall l \in \{1, ..., L\}. \tag{3}$$

Although other data and regularization terms are easily conceivable, we restrict ourselves to these two most popular SP approaches. It was proposed to use the SPDHG method for MPI reconstruction recently as to allow for various different regularization approaches such as FL, classical Tikhonov or ℓ^1 regularization; and still have an algorithm capable of online reconstruction [18]. Moreover, it was shown that the algorithm is highly competitive to the Kaczmarz method. First, the quality of the reconstructed images can be significantly improved by using more suitable or more sophisticated regularization functionals. Second, the computational effort of both algorithms is still comparable when performing a single-patch reconstruction. This is even more important, as the systems we deal with in multi-patch reconstructions are typically huge. Algorithms which cannot challenge the run time of Kaczmarz method in the single patch case will not be able to cope with the by far larger amount of data in the multi-patch setting.

In the following, we describe the SPDHG algorithm in more detail. The algorithm does not solve (3) directly, but instead solves the equivalent saddle-point problem given by

$$\min_{c_l} \quad \max_{y} \langle A c_l, y \rangle - \mathbb{1}_{\{\|y_1\|_\infty \leq 1\}}(y_1) - \langle u_l, y_1 \rangle \tag{4}$$

$$- \mathbb{1}_{\{\|y_2\|_\infty \leq \alpha\}}(y_2) + \beta \|c_l\|_1 + \mathbb{1}_{\{c_l \geq 0\}}(c_l), \tag{5}$$

where $y = (y_1, y_2)^T$ denotes the dual variable, $A = (S, \nabla)^T$ is the stacked linear operator and

$$\mathbb{1}_X(x) = \begin{cases} 0, & x \in X \\ \infty, & \text{else} \end{cases},$$

denotes the indicator function of the set X. In imaging applications, such a saddle point problem is often solved by the Chambolle-Pock algorithm [23], which is computationally expensive for large datasets. The algorithm updates the primal variable and the full dual variable alternately by a proximal operator step. The stochastic variant SPDHG updates only a random part of the dual variable in each iteration and thus is computationally less costly [21]. Instead of splitting the operator and dual variable in two parts belonging to the data term, i.e. the MPI forward operator, and the differential operator, respectively, it is possible to apply additional row-wise splitting to the MPI forward operator. The computationally most expensive steps in the algorithm, matrix-vector multiplications, are then performed on much smaller matrices and thus less expensive. Pseudo code for the single patch SPDHG algorithm can be derived from Algorithm 1 by setting $L = 1$. Details regarding SPDHG implementation and use for MPI reconstruction, e.g. the step size selection, the choice of data splitting, probability distribution and others can be found in [18]. The algorithm is easy to implement and use.

II.I.2. Joint reconstruction

To reduce artifacts near the patches' boundaries we use a joint reconstruction approach. We thus do not solve (1)

 © 2022 Infinite Science Publishing

independently for each patch, but we solve the (sparse) stacked linear system

$$\begin{pmatrix} \tilde{S}_1 \\ \vdots \\ \tilde{S}_L \end{pmatrix} c = \begin{pmatrix} u_1 \\ \vdots \\ u_L \end{pmatrix}, \tag{6}$$

where the matrices $\tilde{S}_1, ..., \tilde{S}_L$ work as $S_1, ..., S_L$ on the part of c, which contains the corresponding patch, and contain zeros everywhere else, i.e. we assume appropriate discrete grids Γ with index set I on Ω^{SF} and Γ_l with index set I_l on Ω_l^{SF}, such that there exist injective mappings $\Phi_l : I_l \to I$ such that

$$\tilde{S}_l = S_l \circ \left(\delta_{\Phi_l(n),m}\right)_{n\in I_l, m\in I}, \tag{7}$$

where δ denotes the Kronecker delta. Denoting $P_l = \left(\delta_{\Phi_l(n),m}\right)_{n\in I_l, m\in I}$, we can thus rewrite (6) as

$$\begin{pmatrix} S_1 \circ P_1 \\ \vdots \\ S_L \circ P_L \end{pmatrix} c = \begin{pmatrix} u_1 \\ \vdots \\ u_L \end{pmatrix}. \tag{8}$$

The standard joint reconstruction approach applies the Kaczmarz method to solve

$$\min_{c\geq 0} \lambda \|c\|_2^2 + \frac{1}{2} \left\|\left((S_l \circ P_l)\, c - u_l\right)_{l=1,...,L}\right\|_2^2. \tag{9}$$

Kaczmarz method operates row-wise and sweeps through all rows in one iteration. Note that the computational effort can be significantly reduced by iterating only over indices $\Phi_l(n)$ for $n \in I_l$ instead of iterating over $n \in I$.

In this paper, we propose to use SPDHG for multi-patch reconstruction. This allows us to apply e.g. total variation regularization, which takes into account neighborhood structures of the voxels across the patches' boundaries. SPDHG can apply row-wise operator splitting and by splitting into $S_1 \circ P_1, ..., S_L \circ P_L$ we can again reduce the computational costs by iterating only over indices $\Phi_l(n)$ for $n \in I_l$.

Moreover, we can apply additional splitting on the data as proposed in [18] using

$$S_l = \left(S_{l,1}, \ldots, S_{l,M}\right)^T, \tag{10}$$

where the matrix is divided into M submatrices by row-wise separation. We call the corresponding M measurement subvectors data batches. Matrix-vector products within the algorithm are then performed on the small matrices $S_{l,m}$. Our approach then solves the minimization problem

$$\min_{c\geq 0} \alpha \mathrm{TV}(c) + \beta \|c\|_1 + \sum_{l=1}^{L} \sum_{m=1}^{M} \left\|\left(S_{l,m} \circ P_l\right) c - u_{l,m}\right\|_1. \tag{11}$$

The resulting algorithm is stated in Algorithm 1.

Algorithm 1 SPDHG for multi-patch MPI reconstruction

input $A = (S, \nabla)^T$, c^0, $y^0 = \left(y_{1,1}^0, ..., y_{L,M}^0, y_{\mathrm{TV}}^0\right)$, $\bar{y}^0$, step sizes $\tau, \sigma > 0$, update probabilities p, parameters α, $\beta > 0$
for k=0,1,2,...,K-1 **do**
  Primal step:
  $c^{k+1} = \mathrm{prox}_{\tau\left(\mathbb{1}_{\{\cdot\geq 0\}}(\cdot) + \beta\|\cdot\|_1\right)}\left(c^k - \tau A^* \overline{y}^k\right)$
  Dual step:
  $y^{k+1} = y^k$
  choose data term or TV term update randomly
  if data term update **then**
    select patch $l \in \{1, ..., L\}$ randomly
    select batch $m \in \{1, ..., M\}$ randomly
    $y_{l,m}^{k+1} = \mathrm{prox}_{\sigma\left(\mathbb{1}_{\{\|\cdot\|_\infty \leq 1\}}(\cdot)\right)}\left(y_{l,m}^k + \sigma\left(S_{l,m} \circ P_l\right) c^{k+1}\right)$
  else
    $y_{\mathrm{TV}}^{k+1} = \mathrm{prox}_{\sigma\left(\mathbb{1}_{\{\|\cdot\|_\infty \leq \alpha\}}(\cdot)\right)}\left(y_{\mathrm{TV}}^k + \sigma \nabla c^{k+1}\right)$
  end if
  Extrapolation step:
  $\overline{y}^{k+1} = y^{k+1} + p^{-1}\left(y^{k+1} - y^k\right)$
end for

II.II. Data

Numerical experiments are first performed on simulated data with simulated system matrices to be able to compare the reconstructions to the ground truth phantom, using measures as the structural similarity index (SSIM) or peak-signal-to-noise-ratio (PSNR). We simulate 2D data in the time domain using the Langevin magnetization model and add Gaussian white noise according to the noise model in [24].

The data are then Fourier transformed and processed as measured data. The scanner is modeled based on the real preclinical MPI system 25/20FF (Bruker BioSpin MRI GmbH, Ettlingen, Germany) at University Medical Center Hamburg-Eppendorf. The drive-field amplitudes are 12 mT in x- and y-direction and the gradient strength is $G_x = G_y = -0.5\,\mathrm{T\,m^{-1}}$. The drive field excitation frequencies are $f_x = 2.5/102$ MHz and $f_y = 2.5/96$ MHz, the repetition time for one Lissajous cycle is $T_R = 652.8\,\mu\mathrm{s}$. To exclude inverse crime, simulations are performed on a ten times finer spatial grid than reconstruction. For reconstruction purposes the voxel size is 2 mm × 2 mm. The SM FOV is of size 66 mm × 66 mm, whereas the drive-field (DF) FOV measures 48 mm × 48 mm. We thus have an overscan of 9 mm in each direction.

For the first phantom, we simulated with an SM FOV overlap but without DF FOV overlap, i.e. the SM center is shifted by 48 mm to obtain the different patches and the phantom which consists of 2×3 patches measures 57×81 voxels. It is depicted in Figure 1 (A) and consists of large homogeneous regions. The drive-field FOV (solid lines) and overscan (dashed) for the upper left patch are indicated in the figure. Further experiments are performed on a sparser phantom, depicted in Figure 1 (B), which is

 © 2022 Infinite Science Publishing

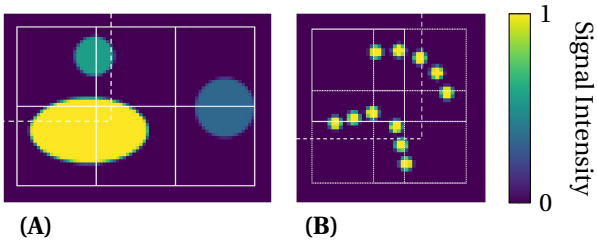

Figure 1: The ellipse phantom (A) and the sparsity phantom (B). For the upper left patch, the DF FOVs are indicated by solid lines and the SM FOVs by dashed lines. DF FOVs for the other patches are indicated by dotted lines for the sparsity phantom.

based on the phantom used in [25]. Following the set-up in [25], the SM centers are shifted by 32 mm resulting in a DF overlap of 16 mm. The full reconstruction grid thus consists of 2×2 patches and measures 49×49 voxels.

To demonstrate the appropriateness of our approach for real data, we use data recorded with the preclinical Bruker MPI system at University Medical Center Hamburg-Eppendorf. The drive-field amplitudes are 12 mT in x- and y-direction with a gradient strength of $-1\,\mathrm{Tm}^{-1}$ in x- and y-direction. The setting consists of 1×2 patches, covering a total SM FOV of 40 mm × 64 mm with each SM covering 40 mm × 40 mm comprising an overscan of 8 mm in each direction. The phantom consists of a bar, which is placed diagonally over the patch intersection. For further details, we refer to [26].

III. Results

We start our experiments by comparing the quality of the reconstructed images for the ellipse phantom. Each algorithm has two parameters to tune (namely α and β for SPDHG and λ and the number of iterations K for Kaczmarz method) and we ran detailed parameter tests.

The best possible SSIM and PSNR values obtained are listed in Table 1. The visually most convincing reconstructions are depicted in Figure 2 and we state the corresponding parameter values.

Single-patch reconstructions lead to boundary artifacts especially visible within the large ellipse. As expected by the choice of regularization, the FL regularized SP reconstructions suffer from less artifacts. However, there are stripe artifacts left. The joint Kaczmarz reconstruction is not able to handle the boundary artifacts due to Tikhonov regularization. Note that the SP Kaczmarz reconstructions have less artifacts and higher SSIM/ PSNR values compared to the joint ones, however, this is due to the smoothing applied by the linear weighting we use to stack the patches. Although this enhances the quality for this specific phantom, it might lead to inferior quality for others. As indicated by the SSIM values, we observe more noise overall in the Kaczmarz reconstructions. The joint SPDHG algorithm outperforms all other reconstruction approaches in terms of quality. It reaches the highest SSIM and PSNR values and leaves no artifacts and almost no noise in the reconstructed images.

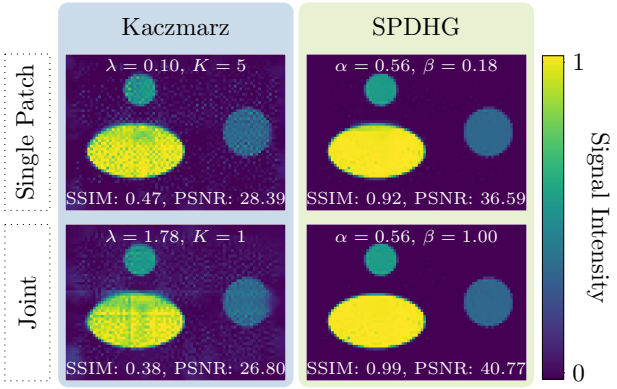

Figure 2: Reconstructed images of the ellipse phantom. Note that the artifacts in the SP Kaczmarz reconstruction are less pronounced than in the joint Kaczmarz reconstruction due to the smoothing applied by the linear weighting we use to stack the patches in the SP case and the very small iteration number in the joint case.

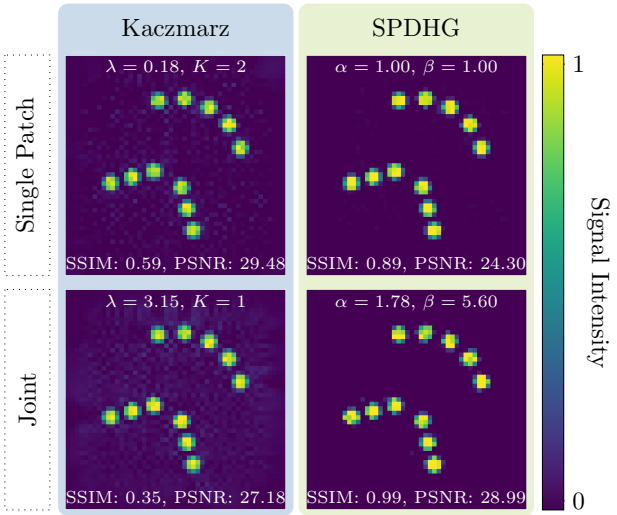

Figure 3: Reconstructed images of the sparsity phantom.

To underline the qualitative enhancement of the reconstructed images, we also compare reconstructions of the sparsity phantom. In this case, we do not expect as much influence of the TV penalty but again we observe a significantly reduced noise level in our reconstructions by SPDHG due to the l^1-penalty term (cf. Figure 3). Again, the best obtained PSNR and SSIM values for the different reconstruction approaches are stated in Table 1 and the corresponding parameter values are stated in the figure. The proposed algorithm again outperforms the Kaczmarz method in terms of both, SSIM and PSNR value.

 © 2022 Infinite Science Publishing

Table 1: Maximum SSIM and PSNR values for different reconstruction approaches for the ellipse and the sparsity phantom.

SP/J	Algorithm	Ellipse phantom		Sparsity phantom	
		max. SSIM	max. PSNR	max. SSIM	max. PSNR
SP	Kaczmarz	0.78	28.39	0.85	29.48
SP	SPDHG	0.92	36.59	0.95	24.30
J	Kaczmarz	0.61	26.80	0.52	27.18
J	SPDHG	**0.99**	**40.77**	**0.99**	**30.75**

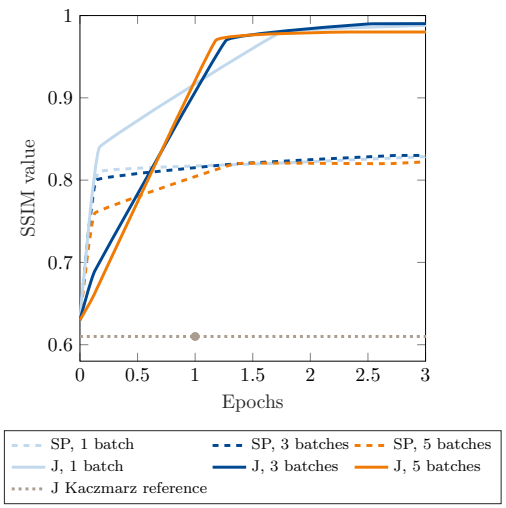

Figure 4: The SSIM value of reconstructed images of the ellipse phantom against the run time in joint Kaczmarz epochs for different amounts of additional data splitting for single patch and joint SPDHG. The SSIM values reached by joint Kaczmarz is indicated as a reference value.

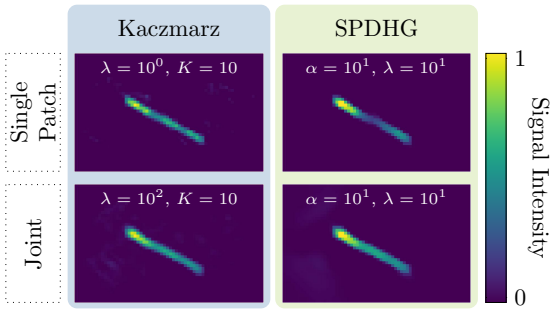

Figure 5: Reconstructed images of measured data of the 2-patch bar phantom.

We now compare the run times of the different algorithms. As one epoch, we define the time it takes to run one iteration of the joint Kaczmarz algorithm. When using SPDHG, we study the influence of additional data splitting as in (10) on the run time and the quality of the reconstructed images. For these experiments, we use the six patches ellipse phantom. Note that our standard setting for the joint approach is the use of six data batches corresponding to the six patches and explicitly mentioned splitting means on top of that. We compare the SSIM values reached after a fixed number of epochs for single-patch approach and joint approach using the example of the ellipse phantom reconstruction in Figure 4. Both, SP and joint SPDHG surpass the maximum SSIM value reached by joint Kaczmarz almost immediately. SP Kaczmarz reaches a higher SSIM value than joint Kaczmarz (i.e. 0.78 compared to 0.61), but this is reached mostly due to the smoothing by our stacking approach. Still, also the maximum SSIM value obtained by SP Kaczmarz is surpassed by all SPDHG approaches after approximately half an epoch. After less than one epoch, all joint SPDHG algorithms reach a higher SSIM value than SP SPDHG does at maximum. We further note that additional data splitting has limited influence in the multi-patch setting. Three data batches are sufficient to reach the maximum image quality after approximately one epoch, such that early stopping could be applied at that point. However, we expect that even higher influence of data splitting might be possible as we suspect the limited influence might be caused by the implementation of the algorithms, which need the more frequent storage accesses to suboptimal data types the more splitting is applied. Moreover, please note that all algorithms are not implemented in parallel although SPDHG is highly parallelizable.

With the help of simulated data, we were able to survey the results of the proposed method by comparison to a ground truth. We underline the promising findings by reconstruction of measured data in order to show the applicability of the method. The reconstructed images for the different approaches can be seen in Figure 5. Note that we used TV and ℓ^2 regularization for the SPDHG reconstructions instead of FL regularization as that seems to better fit the data and additionally underlines the flexibility of the scheme. As we have seen for simulated data, the Kaczmarz reconstructions suffer from more noise artifacts than the SPDHG ones. Moreover, the images reconstructed by the SP approaches face severe boundary artifacts with more severe artifacts in the SPDHG reconstructed image. The joint approaches significantly reduce those artifacts with joint SPDHG achieving the most homogeneous concentration within the patch boundary region.

 © 2022 Infinite Science Publishing

IV. Discussion

The quality of reconstructed multi-patch MPI images can be significantly improved by choosing an appropriate regularization term and a suitable norm for the data fitting term. Our experiments underline the benefits of regularizations, which take into account neighborhood structures within the images and especially across patches' boundaries. Reconstructions obtained by using TV regularization outperform the current state-of-the art reconstructions in terms of SSIM and PSNR value as well as by visual inspection.

Our numerical experiments show that the SPDHG algorithm allows for such regularization terms while preserving a short run time. The exemplary SPDHG algorithm for FL regularization is competitive to joint Kaczmarz concerning the run time and effort for parameter tuning. In summary, the SPDHG algorithm comes with similar computational costs compared to the Kaczmarz method but provides the opportunity to significantly improve the quality of the reconstructed images.

We expect even better performance when implemented with appropriate data structures and in parallel. The short run time allows for reconstruction of 40 patches and more within decent time, which makes the approach relevant for application in practice. Moreover, there are potential savings in calibration time and memory consumption by the neighborhood respecting regularization.

Acknowledgments

The authors would like to thank Konrad Scheffler for sharing his data and providing help in processing it.

C.B. acknowledges the support by the Deutsche Forschungsgemeinschaft (DFG) within the Research Training Group GRK 2583 "Modeling, Simulation and Optimization of Fluid Dynamic Applications".

References

[1] J. Rahmer, J. Weizenecker, B. Gleich, and J. Borgert. Signal encoding in magnetic particle imaging: properties of the system function. *BMC Medical Imaging*, 9:4, 2009, doi:10.1186/1471-2342-9-4.

[2] J. Bohnert and O. Dössel, Calculation and evaluation of current densities and thermal heating in the body during MPI, in *Magnetic Nanoparticles*, 162–168, World Scientific, 2010. doi:10.1142/9789814324687_0023.

[3] E. U. Saritas, P. W. Goodwill, G. Z. Zhang, and S. M. Conolly. Magnetostimulation Limits in Magnetic Particle Imaging. *IEEE Transactions on Medical Imaging*, 32(9):1600–1610, 2013, doi:10.1109/TMI.2013.2260764.

[4] I. Schmale, B. Gleich, J. Rahmer, C. Bontus, J. Schmidt, and J. Borgert. MPI Safety in the View of MRI Safety Standards. *IEEE Transactions on Magnetics*, 51(2):1–4, 2015, doi:10.1109/TMAG.2014.2322940.

[5] M. Ahlborg, C. Kaethner, T. Knopp, P. Szwargulski, and T. M. Buzug. Using data redundancy gained by patch overlaps to reduce truncation artifacts in magnetic particle imaging. *Physics in Medicine and Biology*, 61(12):4583–4598, 2016, doi:10.1088/0031-9155/61/12/4583.

[6] M. Grüttner, T. F. Sattel, M. Graeser, H. Wojtczyk, G. Bringout, W. Tenner, and T. M. Buzug, Enlarging the Field of View in Magnetic Particle Imaging – A Comparison, in *Magnetic Particle Imaging*, 2012, 249–253. doi:10.1007/978-3-642-24133-8_40.

[7] T. Knopp, K. Them, M. Kaul, and N. Gdaniec. Joint reconstruction of non-overlapping magnetic particle imaging focus-field data. *Physics in Medicine and Biology*, 60(8):L15–L21, 2015, doi:10.1088/0031-9155/60/8/L15.

[8] P. Szwargulski, M. Möddel, N. Gdaniec, and T. Knopp. Efficient Joint Image Reconstruction of Multi-Patch Data Reusing a Single System Matrix in Magnetic Particle Imaging. *IEEE Transactions on Medical Imaging*, 38(4):932–944, 2019, doi:10.1109/TMI.2018.2875829.

[9] M. Boberg, T. Knopp, P. Szwargulski, and M. Moddel. Generalized MPI Multi-Patch Reconstruction Using Clusters of Similar System Matrices. *IEEE Transactions on Medical Imaging*, 39(5):1347–1358, 2020, doi:10.1109/TMI.2019.2949171.

[10] C. Brandt and A. Seppänen. Recovery from Errors Due to Domain Truncation in Magnetic Particle Imaging: Approximation Error Modeling Approach. *Journal of Mathematical Imaging and Vision*, 60(8):1196–1208, 2018, doi:10.1007/s10851-018-0807-z.

[11] J. Lampe, C. Bassoy, J. Rahmer, J. Weizenecker, H. Voss, B. Gleich, and J. Borgert. Fast reconstruction in magnetic particle imaging. *Physics in Medicine and Biology*, 57(4):1113–1134, 2012, doi:10.1088/0031-9155/57/4/1113.

[12] T. Knopp, J. Rahmer, T. F. Sattel, S. Biederer, J. Weizenecker, B. Gleich, J. Borgert, and T. M. Buzug. Weighted iterative reconstruction for magnetic particle imaging. *Physics in Medicine and Biology*, 55(6):1577–1589, 2010, doi:10.1088/0031-9155/55/6/003.

[13] F. Lieb and T. Knopp. A wavelet-based sparse row-action method for image reconstruction in magnetic particle imaging. *Medical Physics*, 48(7):3893–3903, 2021, doi:10.1002/mp.14938.

[14] C. Bathke, T. Kluth, C. Brandt, and P. Maaß. Improved image reconstruction in magnetic particle imaging using structural a priori information. *International Journal on Magnetic Particle Imaging*, 3(1), 2017, doi:10.18416/IJMPI.2017.1703015.

[15] S. Ilbey, C. B. Top, T. Cukur, E. U. Saritas, and H. E. Guven, Image reconstruction for Magnetic Particle Imaging using an Augmented Lagrangian Method, in *2017 IEEE 14th International Symposium on Biomedical Imaging (ISBI 2017)*, 64–67, IEEE, 2017. doi:10.1109/ISBI.2017.7950469.

[16] M. Maass, C. Droigk, F. Katzberg, P. Koch, and A. Mertins, A Recovery Algorithm based on the Kaczmarz Algorithm and ADMM Splitting with Application to Convex Optimization in Magnetic Particle Imaging, in *2020 28th European Signal Processing Conference (EUSIPCO)*, 2135–2139, IEEE, 2021. doi:10.23919/Eusipco47968.2020.9287487.

[17] M. Storath, C. Brandt, M. Hofmann, T. Knopp, J. Salamon, A. Weber, and A. Weinmann. Edge Preserving and Noise Reducing Reconstruction for Magnetic Particle Imaging. *IEEE Transactions on Medical Imaging*, 36(1):74–85, 2017, doi:10.1109/TMI.2016.2593954.

[18] L. Zdun and C. Brandt. Fast MPI reconstruction with non-smooth priors by stochastic optimization and data-driven splitting. *Physics in Medicine & Biology*, 66(17):175004, 2021, doi:10.1088/1361-6560/ac176c.

[19] L. Condat. A Primal–Dual Splitting Method for Convex Optimization Involving Lipschitzian, Proximable and Linear Composite Terms. *Journal of Optimization Theory and Applications*, 158(2):460–479, 2013, doi:10.1007/s10957-012-0245-9.

[20] A. Beck and M. Teboulle. Fast Gradient-Based Algorithms for Constrained Total Variation Image Denoising and Deblurring Prob-

 © 2022 Infinite Science Publishing

lems. *IEEE Transactions on Image Processing*, 18(11):2419–2434, 2009, doi:10.1109/TIP.2009.2028250.

[21] A. Chambolle, M. J. Ehrhardt, P. Richtárik, and C.-B. Schönlieb. Stochastic Primal-Dual Hybrid Gradient Algorithm with Arbitrary Sampling and Imaging Applications. *SIAM Journal on Optimization*, 28(4):2783–2808, 2018, doi:10.1137/17M1134834.

[22] L. Zdun, M. Boberg, and C. Brandt. Fast and artifact reducing joint multi-patch MPI reconstruction. *International Journal on Magnetic Particle Imaging*, 8(1 Suppl. 1), 2022, doi:10.18416/IJMPI.2022.2203042.

[23] T. Pock, D. Cremers, H. Bischof, and A. Chambolle, An algorithm for minimizing the Mumford-Shah functional, in *2009 IEEE 12th International Conference on Computer Vision*, 1133–1140, IEEE, 2009. doi:10.1109/ICCV.2009.5459348.

[24] J. Weizenecker, J. Borgert, and B. Gleich. A simulation study on the resolution and sensitivity of magnetic particle imaging. *Physics in Medicine and Biology*, 52(21):6363–6374, 2007, doi:10.1088/0031-9155/52/21/001.

[25] N. Gdaniec, M. Boberg, M. Moddel, P. Szwargulski, and T. Knopp. Suppression of Motion Artifacts Caused by Temporally Recurring Tracer Distributions in Multi-Patch Magnetic Particle Imaging. *IEEE Transactions on Medical Imaging*, 39(11):3548–3558, 2020, doi:10.1109/TMI.2020.2998910.

[26] K. Scheffler, M. Boberg, and T. Knopp. Boundary artifact reduction by extrapolating system matrices outside the field-of-view in joint multi-patch MPI. *International Journal on Magnetic Particle Imaging*, 8(1 Suppl. 1), 2022, doi:10.18416/IJMPI.2022.2203019.

 © 2022 Infinite Science Publishing